Perfusion-Dependent Cerebral Autoregulation Impairment in Hemispheric Stroke

Nils Hecht, MD [iD],[1,2] Max Schrammel, MD,[1,2,3] Konrad Neumann, PhD,[4]
Marc-Michael Müller, MD,[1,2,5] Jens P. Dreier, MD [iD],[2,6,7,8,9] Peter Vajkoczy, MD,[1,2]
and Johannes Woitzik, MD[1,2,3]

Objective: Loss of cerebral autoregulation (CA) plays a key role in secondary neurologic injury. However, the regional distribution of CA impairment after acute cerebral injury remains unclear because, in clinical practice, CA is only assessed within a limited compartment. Here, we performed large-scale regional mapping of cortical perfusion and CA in patients undergoing decompressive surgery for malignant hemispheric stroke.

Methods: In 24 patients, autoregulation over the affected hemisphere was calculated based on direct, 15 to 20-minute cortical perfusion measurement with intraoperative laser speckle imaging and mean arterial blood pressure (MAP) recording. Cortical perfusion was normalized against noninfarcted tissue and 6 perfusion categories from 0% to >100% were defined. The interaction between cortical perfusion and MAP was estimated using a linear random slope model and Pearson correlation.

Results: Cortical perfusion and CA impairment were heterogeneously distributed across the entire hemisphere. The degree of CA impairment was significantly greater in areas with critical hypoperfusion (40–60%: 0.42% per mmHg and 60–80%: 0.46% per mmHg) than in noninfarcted (> 100%: 0.22% per mmHg) or infarcted (0–20%: 0.29% per mmHg) areas (*$p < 0.001$). Pearson correlation confirmed greater CA impairment at critically reduced perfusion (20–40%: $r = 0.67$; 40–60%: $r = 0.68$; and 60–80%: $r = 0.68$) compared to perfusion > 100% ($r = 0.36$; *$p < 0.05$). Tissue integrity had no impact on the degree of CA impairment.

Interpretation: In hemispheric stroke, CA is impaired across the entire hemisphere to a variable extent. Autoregulation impairment was greatest in hypoperfused and potentially viable tissue, suggesting that precise localization of such regions is essential for effective tailoring of perfusion pressure-based treatment strategies.

ANN NEUROL 2021;89:358–368

Cerebral autoregulation (CA) is defined as the intrinsic capacity of cerebral vasculature to maintain constant cerebral blood flow (CBF) within physiological ranges of cerebral perfusion pressure (CPP).[1,2] Impaired CA with more or less zero-slope relationship between CPP and CBF has previously been reported in various settings of acute brain injury and is associated with an increased risk of secondary neurologic injury.[3–6] To individually detect and react to secondary neurological worsening, continuous bed-side assessment of CA in real-time has meanwhile been established as extended monitoring in neurointensive care.[7,8] In this context, dynamic CA describes the real-

time CBF response to changes in blood pressure (BP) using continuous monitoring techniques and time-correlation methods,[9] where CPP is recorded together with regional CBF,[10] middle cerebral artery (MCA) flow velocity,[11] near-infrared spectroscopy,[12] or brain tissue partial pressure of oxygen (ptiO$_2$).[13]

At present, assessment and interpretation of CA remains limited by 2 main factors: (1) techniques for continuous CA assessment mainly rely on surrogate cerebral perfusion markers, and (2) each technique only permits CA assessment within a small cerebral tissue sample. In acute cerebral injury, this is problematic because the regional distribution and degree of CA impairment may vary depending on the extent and severity of the underlying (ischemic) injury. In patients with large hemispheric infarction, for example, it was shown that CA impairment can occur in nonischemic tissue neighboring the infarct but also in areas more remote.[6,14] The cause for this seemingly random distribution pattern remains unknown but the occurrence and degree of CA impairment could be influenced by the underlying perfusion level within the affected tissue, because hypoperfusion with metabolic compromise represent triggers of CA impairment.[6] Thus, a more differentiated approach toward CA assessment based on a comprehensive regional understanding of CA may help optimize BP-guided treatment decisions aiming to prevent secondary neurological injury.[8,15–17]

Patients requiring surgery for malignant hemispheric stroke (MHS) represent an ideal population to investigate the pathophysiology of CA, because surgical decompression exposes a large proportion of the affected hemisphere. This offers the unique opportunity for dynamic and direct real-time measurement of cortical perfusion above a large surface area of the human brain using noninvasive optical blood flow imaging. Here, others and our group have previously shown the feasibility and validity of intraoperative laser speckle imaging (iLSI) based on dynamic light scattering off moving particles, mainly erythrocytes.[18–23] In the present study, we used continuous iLSI for large-scale, real-time cortical perfusion mapping and offline CA assessment in patients undergoing decompressive hemicraniectomy (DC) for MHS.

Methods

Study Design and Patient Population

This prospective observational study was approved by the ethics committee of the Charité-Universitätsmedizin Berlin, Germany (EA4/109/07) and performed in compliance with Health Insurance Portability and Accountability Act regulations. Between July 2009 and January 2013, 24 patients who underwent DC for treatment of space-occupying MCA infarction with the risk of malignant edema development were included after informed consent was obtained. To determine the association between spontaneous fluctuations in BP and changes in CBF, cortical perfusion above the affected hemisphere and mean arterial blood pressure (MAP) were recorded for 15 to 20 minutes in each patient using noninvasive iLSI and arterial BP monitoring. The degree of cortical autoregulation impairment was estimated based on the interaction between spontaneous MAP fluctuations and changes in cortical perfusion. The initial neurological deficit was assessed using the Glasgow Coma Scale (GCS) and modified National Institutes of Health Stroke Scale (mNIHSS). Outcome at 12 months was determined according to the modified Rankin Scale score (mRS). Demographic, clinical, and radiographic patient data were retrospectively analyzed by a clinician who was not directly involved in the patients' care.

Patient Management

Treatment was performed according to the guidelines of the German Society of Neurosurgery. "Malignant" MCA infarction and the indication for surgery was defined according to the uniform inclusion criteria of the 4 randomized controlled trials on hemicraniectomy, DECIMAL, DESTINY I, DESTINY II, and HAMLET.[24,25] Exclusion criteria, such as premorbid mRS >1, premorbid Barthel Index < 95, other concomitant severe disease that would confound with treatment, or life expectancy < 3 years were not applied. Decompressive hemicraniectomy was performed as previously described.[26–28] During surgery, all patients were anesthetized with propofol and remifentanil and received a bodyweight-adapted dose of 50 mg/kg mannitol 30 minutes before skin incision, according to our institutional guidelines. Mean arterial BP was targeted at 80 to 90 mmHg and coregistered during the iLSI perfusion measurement. The end-expiratory carbon dioxide concentration during surgery was maintained at a level corresponding to an arterial partial pressure of carbon dioxide between 38 and 42 mmHg. Postoperatively, patients were transferred to our neurointensive care unit. Intracranial pressure (ICP) was continuously monitored and patients remained intubated and sedated until ICP was within normal ranges. A critical ICP threshold was defined as ICP >20 mmHg for longer than 10 minutes and treated with cerebrospinal fluid drainage, osmotic therapy, and deep sedation. Blood gases, electrolytes, and glucose were controlled every 4 hours. A routine postoperative computerized tomography (CT) or magnetic resonance imaging (MRI) scan was performed within 24 hours after surgery to rule out procedure-related complications.

Neuroimaging Analysis

Neuroimaging characteristics shown in the Table were determined from CT or matched diffusion weighted imaging (DWI) and fluid attenuated inversion recovery (FLAIR) sequences of MRI sequences. In a subgroup of 19 patients with available postoperative MRI, the cortical extent of the infarcted tissue was superimposed onto the laser speckle perfusion maps based on the cortical surface anatomy, as previously described.[21] Significant hemodynamic mismatch at the timepoint of MRI was excluded by perfusion-diffusion mismatch analysis. Perfusion-weighted imaging was performed with a serial T2* weighted single-shot gradient echo-planar imaging sequence. Gadolinium-contrast agent (0.1 mmol/kg bodyweight; Magnevist; Schering) was injected as a bolus rate of 4 to 6 mL/second. Volumetric analysis was performed with image guidance software (Brainlab Cranial Planning SmartBrush version 2.6.0.121; Brainlab AG, Munich, Germany, and Visage Imaging 7, Visage Imaging, Berlin, Germany). Volume gain was calculated as ipsilateral volume minus contralateral volume. Swelling was determined as volume gain divided by contralateral volume. Volume of infarction corrected for swelling was calculated as volume of infarction divided by swelling plus 1.

Intraoperative Laser Speckle Imaging

After craniotomy and durotomy, a laser speckle imager (MoorFLPI; Moor Instruments Ltd., Axminster, UK) was positioned perpendicular over the infarcted hemisphere with a distance of 300 mm. The total exposed surface area (A), as shown in the Table, was estimated based on the spherical length (a = major radius) and width (b = minor radius) of the bone flap according to the following:

$$A = a \times b \times \pi$$

Cortical perfusion in the arbitrary perfusion unit CBF-Flux was recorded within an 18×24 cm imaging field over the exposed cortical hemisphere with purpose designed data acquisition software (MoorFLPI measurement software, version V3.0; Moor Instruments Ltd.) for 15 to 20 minutes at 25 Hz using a temporal filter of 100 frames per image to allow optimal spatial resolution (760×568 pixel, exposure time 8.4 ms) and minimize potential motion artifacts.[19,21] This resulted in an actual image acquisition rate of 0.25 Hz and 225 to 300 consecutive laser speckle perfusion maps. Identical focal lens settings and exposure times were maintained during all measurements. Direct illumination of the surgical field by light sources other than the laser was avoided. Corresponding MAP levels were recorded at 0.02 Hz (Fig 1).

Data Processing of Laser Speckle Perfusion Maps

The iLSI blood flow maps were analyzed by positioning polygonal regions of interest (ROIs) within the entire area of the surgically exposed imaging field under exclusion of the large surface vasculature (MoorFLPI review software, version V3.0; Moor Instruments Ltd.). Within each ROI and patient, a pixel-by-pixel calculation of arbitrary cortical perfusion expressed as CBF-Flux was performed to determine the mean perfusion in each ROI. Next, CBF-Flux above the entire hemisphere was normalized against the mean CBF-Flux within the suspected noninfarcted territory, which we defined as 100% based on the mean CBF-Flux that we recorded within that region.[19,21]

Perfusion-Based Autoregulation Assessment

The algorithm for perfusion-based autoregulation assessment is illustrated in Figure 2. After normalization, 6 categories of cortical perfusion ranging from 0% to >100% were defined and a maximum of 10 polygonal ROIs were positioned above the parenchymal areas corresponding to each of the 6 perfusion categories. Next, cortical perfusion within each ROI and perfusion category was calculated for the 15 to 20-minute LSI recording period to estimate the interaction between MAP fluctuations and changes in cortical perfusion.

In addition, the degree of CA impairment for each perfusion level was assessed by Pearson correlation. In a subgroup of 19 patients, ROIs from critical perfusion levels 40 to 60% and 60 to 80% were categorized according to their location within infarcted or noninfarcted tissue to determine the relevance of the tissue viability on the degree of CA impairment.

Statistical Analysis

The sample size was based on availability. Of all the patients that were included in our prospective MHS neuromonitoring trial, 33 underwent iLSI. Of these, 9 patients were excluded from CA analysis due to an incomplete (n = 2) iLSI data set, unavailability of coregistered BP (n = 5), or a temporal filter set at zero instead of 100 frames per second (n = 2). Descriptive summary statistics are presented as mean ± standard deviation (SD) or median and range (minimum – maximum), as appropriate. Means, standard errors (SEs), and 2-sided 95% confidence intervals (95% CIs) of the interaction between MAP fluctuations and changes in CBF-Flux were estimated from a random slope model. The linear model equation of the linear random slope model was MAP, and the perfusion category and the interaction of both variables were as fixed effects. In addition to the fixed effects, the model contained a random intercept and MAP (random slope) as random effects, which model individual

TABLE. Demographic and Clinical Patient Data

No.	Age, sex	Initial GCS/ mNIHSS	Location	Time to surgery, h	Exposed cortical surface, cm^2	Vol. of infarction, cm^3	Vol. gain, cm^3	Swelling, %	Vol. of infarction, corrected, cm^3	12-mo mRS
1	59, M	15/18	MCA / PCA (R)	29	188	528	179	30	407	4
2	62, M	9/20	MCA (L)	14	219	352	78	14	310	6
3	59, M	14/14	MCA (R)	46	272	217	73	13	191	3
4	43, F	13/16	MCA (R)	25	196	211	78	16	181	3
5	59, F	11/17	MCA / ACA (L)	47	179	363	90	22	299	4
6	29, M	4/22	MCA / ACA (L)	8	220	494	130	21	409	6
7	49, M	15/19	MCA / PCA (R)	18	212	380	109	20	316	4
8	44, M	14/12	MCA (R)	36	221	370	163	26	293	5
9	72, F	13/16	MCA / ACA / PCA (L)	29	159	377	117	24	305	6
10	44, M	15/14	MCA (R)	36	182	261	70	14	228	2
11	82, F	12/20	MCA / PCA (R)	18	165	356	108	23	291	6
12	48, F	8/12	MCA / ACA / PCA (L)	32	188	372	48	10	337	6
13	68, M	12/15	MCA / ACA (R)	29	225	407	136	23	332	4
14	47, M	13/12	MCA / ACA / PCA (R)	14	198	643	226	42	452	5
15	70, M	12/16	MCA / ACA (R)	31	232	680	249	42	479	5
16	74, F	13/21	MCA / ACA (R)	24	N/A	415	76	14	363	6
17	60, M	14/10	MCA (R)	44	229	352	128	23	286	6
18	52, F	15/21	MCA (R)	30	201	188	89	18	159	3
19	63, F	12/17	MCA / ACA / PCA (R)	20	195	443	75	16	383	5
20	50, M	10/19	MCA (L)	46	209	300	116	21	249	4
21	57, M	8/18	MCA (L)	45	206	303	118	22	249	4
22	72, M	15/13	MCA (R)	36	191	378	189	38	274	4
23	60, M	13/11	MCA (R)	24	178	399	162	26	316	4
24	68, F	12/15	MCA / ACA / PCA (R)	31	N/A	442	95	16	381	4
	59 (29–82)	13 (4–15)/16 (10–22)		29.5 (8–47)	203 ± 25.3	385 ± 118.8	121 ± 51.1	22 ± 8.5	312 ± 81.4	4 (2–6)

ACA = anterior cerebral artery; F = female; GCS = Glasgow Coma Scale score; h = hours; L = left; M = male; MCA = middle cerebral artery; mNIHSS = modified National Institutes of Health Stroke Scale; mRS = modified Rankin Scale score; N/A = not available; PCA = posterior cerebral artery; R = right; Vol. = volume.

deviation from the mean structure. The multiple level of significance was α = 0.05. The level of significance for each comparison of the mean slopes depending on the perfusion category was Bonferroni adjusted to α = 0.003. The degree of autoregulation impairment for each perfusion category and between infarcted and noninfarcted surface areas was characterized by Pearson correlation and compared by 1-way analysis of variance or a paired Student's *t* test. Statistics were performed with GraphPad Prism for Mac (version 8.4.1; GraphPad Software, San Diego, CA) and R (version 3.5.0; The R Foundation for Statistical Computing, Vienna, Austria).

Results

Demographic, clinical, and radiographic data are presented in the Table . The mean individually exposed cortical surface area was determined at 203 ± 25.3 cm^2. BP during the recording period is illustrated in Figure 3. For each perfusion category, 578 (577 for ">100%") polygonal ROIs were analyzed across all hemispheres during the entire iLSI recording period. In patients number 2, 7, 9, and 16, we observed hemodynamic propagation patterns of spontaneous spreading depolarization across 5.7 cm^2, 3.7 cm^2, 5.5 cm^2, and 4.5 cm^2 of the exposed cortical surface area.

The degree of autoregulation impairment was estimated with a random linear slope model (Fig 4A) with the interaction between MAP and CBF-Flux serving as a proportional measure. As a first sign of a globally impaired autoregulation, we observed that a linear cortical perfusion change (%) per mmHg change in MAP did in fact occur across all levels of perfusion. However, this linear cortical perfusion change (expressed as the slope of the regression lines) differed significantly depending on the underlying level of perfusion and was significantly greater in regions with critically reduced perfusion ("40–60%" $\frac{0.42\%}{mmHg}$ and "60–80%" $\frac{0.46\%}{mmHg}$) compared to areas with higher (">100%" $\frac{0.22\%}{mmHg}$ and "80–100%" $\frac{0.32\%}{mmHg}$) or lower ("0–20%" $\frac{0.29\%}{mmHg}$ and "20–40%" $\frac{0.33\%}{mmHg}$) perfusion levels (*$p < 0.001$ for each comparison; Fig 4B), suggesting a greater autoregulation impairment in areas with hypoperfused "penumbral" perfusion compared to regions of likely noninfarcted or infarcted tissue. To express the degree of autoregulation impairment using a more widely applied measure of cerebral autoregulation, CBF-Flux and MAP were additionally calculated as linear Pearson correlation coefficients[6,15,29] and $r > 0.4$ was defined as the threshold for "severe" impairment.[30] In line with our findings above, linear Pearson correlation confirmed significantly greater autoregulation impairment in areas with

critically reduced but not definitely infarcted cortical perfusion ("20–40%" $r = 0.67$; "40–60%" $r = 0.68$; and "60–80%" $r = 0.68$) compared to regions with likely noninfarcted tissue (">100%" $r = 0.36$; *$p < 0.05$ for each comparison; Fig 5). In regions with critically reduced perfusion levels and greatest CA impairment, the underlying tissue viability had no impact on the degree of CA impairment (Fig 6).

Discussion

For the first time, we directly demonstrate that autoregulation in hemispheric stroke is impaired across the entire affected hemisphere and that CA impairment occurs to a variable degree. Importantly, this degree was influenced by the underlying cortical perfusion level and greatest in regions of hypoperfused but still potentially viable tissue. Together, this highlights that localization of such regions may be essential for effective management of CPP-targeted treatment strategies.

Methodology for Cerebral Perfusion and CA Assessment

In patients with large ischemic stroke, longitudinal tracking of pathophysiological changes is essential to individually detect and react to secondary neurological worsening. In this context, monitoring and assessment of cerebral perfusion and CA may be useful for personalized targeting of cerebral perfusion management goals, determination of the response to interventions, and prognostication.[15,31] In neurocritical care, CBF or surrogate CBF parameters for CA assessment can be continuously measured with minimally invasive regional CBF or ptiO$_2$ microprobes.[32,33] However, this technology only provides information on a very limited tissue compartment, which may lead to misinterpretation and under-representation of the global cerebral perfusion. In the present study, the large surgical exposure presented a unique opportunity to map and characterize the pathophysiological cortical (parenchymal) perfusion response to systemic BP fluctuations in high spatial–temporal resolution using noninvasive LSI. In the context of CA assessment in an experimental rodent model, LSI was shown to reliably determine the perfusion response to BP changes within and beyond the physiological limits of CA.[34] Importantly, iLSI is characterized by a dynamic response sensitivity even to minor flow changes[19,20,35] and able to categorize perfusion thresholds that correspond to eventually infarcted and noninfarcted tissue in the human brain.[21] This allowed us to define different cortical perfusion levels across the entire affected hemisphere according to likely infarcted, penumbral, or noninfarcted tissue.
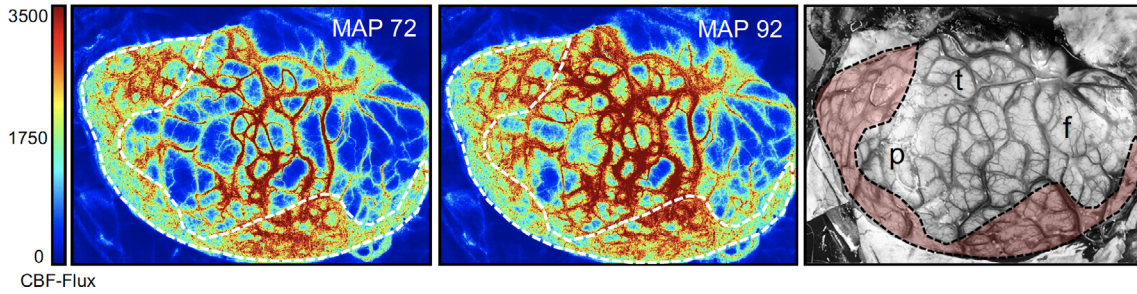
Laser Speckle perfusion maps

FIGURE 1: Intraoperative laser speckle perfusion maps of the left cortical surface after hemicraniectomy and opening of the dura. Arbitrary perfusion is calculated in CBF-Flux ranging from 0 to 3500 and visualized in a color-coded perfusion map. Snapshots of the LSI perfusion recording taken at a mean arterial pressure (MAP) of 72 mmHg (*left image*) and 92 mmHg (*center image*) show a visible perfusion change. The dashed area illustrates the region of suspected undisturbed cortical perfusion. The right image shows a corresponding photograph of the exposed cortical surface with overlay of potentially undisturbed cortical perfusion area. CBF = cerebral blood flow; f = frontal; LSI = laser speckle imaging; p = parietal; t = temporal.

For calculation and estimation of CA, there is currently no widely accepted "best choice."[15] In the present study, we performed a time-correlated CA estimation, because the direct association between pressure and cerebral perfusion represents the most fundamental concept of cerebrovascular autoregulation and can be helpful to guide treatment decisions and predict outcome.[36] Importantly, time-correlation represents the most frequently used CA assessment tool in neurointensive care, because neuromonitoring permits continuous assessment of (surrogate) cerebral perfusion. Therefore, we believe that our findings can be directly translated to neurointensive care, where dynamic CA cannot be recorded in high regional resolution. The fact that MAP was chosen as a parameter for "pressure" instead of CPP is explained by the fact that

only a small fraction of our patients required pre- or intraoperative placement of an external ventricular drain or intracranial pressure probe. However, this also presents a limitation that needs to be addressed, because we naturally cannot exclude that to some extent the variable cerebrovascular occlusion pattern in our patients may have influenced the degree of the cerebral perfusion change in response to the spontaneous BP fluctuations.

Perfusion-Dependent Autoregulation in Ischemic Stroke

BP management remains one of the most essential therapeutic targets for dynamic optimization of cerebral perfusion but the ideal BP level particularly in the acute phase of large vessel occlusion is unclear. Both very high and
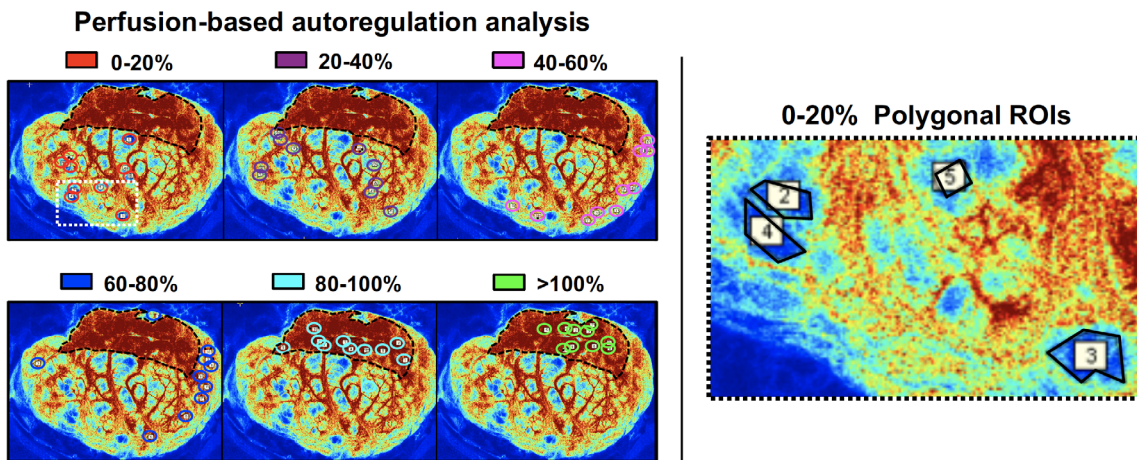
Perfusion-based autoregulation analysis

FIGURE 2: For perfusion-based autoregulation assessment, arbitrary perfusion (CBF-Flux) was first normalized against the mean CBF-Flux within the region of potentially noninfarcted tissue, defined as 100% (dashed area). Next, 6 categories of cortical perfusion ranging from 0% to >100% were defined and 10 polygonal regions of interest (ROIs) were positioned above parenchymal areas corresponding to each of the 6 perfusion categories (*left panels*; for the purpose of visualization, the polygonal ROIs for each of the 6 categories were circled in 6 different colors). The image on the right shows a magnification of the inlay in the 0 to 20% perfusion category and depicts the shape and placement of 3 polygonal ROIs in this perfusion category. During the 15 to 20-minute LSI measurement, cortical perfusion was recorded within each ROI for estimation of the interaction with corresponding mean arterial blood pressure using a linear random slope model and Pearson correlation analysis. CBF = cerebral blood flow; LSI = laser speckle imaging.
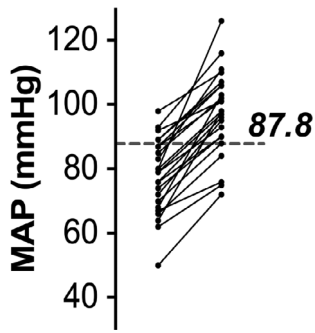
FIGURE 3: Line graph showing the range of spontaneous blood pressure fluctuation during the laser speckle recording period in each patient. The dashed gray line illustrates the overall mean arterial blood pressure (MAP).

depending on the degree of CA impairment, optimal CPP may differ widely.[39,40] Against this background, our findings suggest that this corridor of optimal CPP may even differ within and not just between affected individuals, because the degree and regional distribution of autoregulation impairment that we observed was highly heterogenous. Specifically, CA impairment was greatest in regions with critically reduced perfusion and linked to the underlying perfusion level, which appeared to be heterogeneously distributed across the exposed cortical surface. Interestingly, regions with critically reduced perfusion and greatest CA impairment were not visually tied to the core of the infarct but highly variable in size and location, as illustrated in Figure 2. Clinically, this observation is highly relevant because it shows that bedside placement of neuromonitoring probes roughly in the penumbra of the ischemic core or directly next to the noninfarcted tissue border may not accurately reflect the regions with the highest risk of secondary neurologic injury based on their
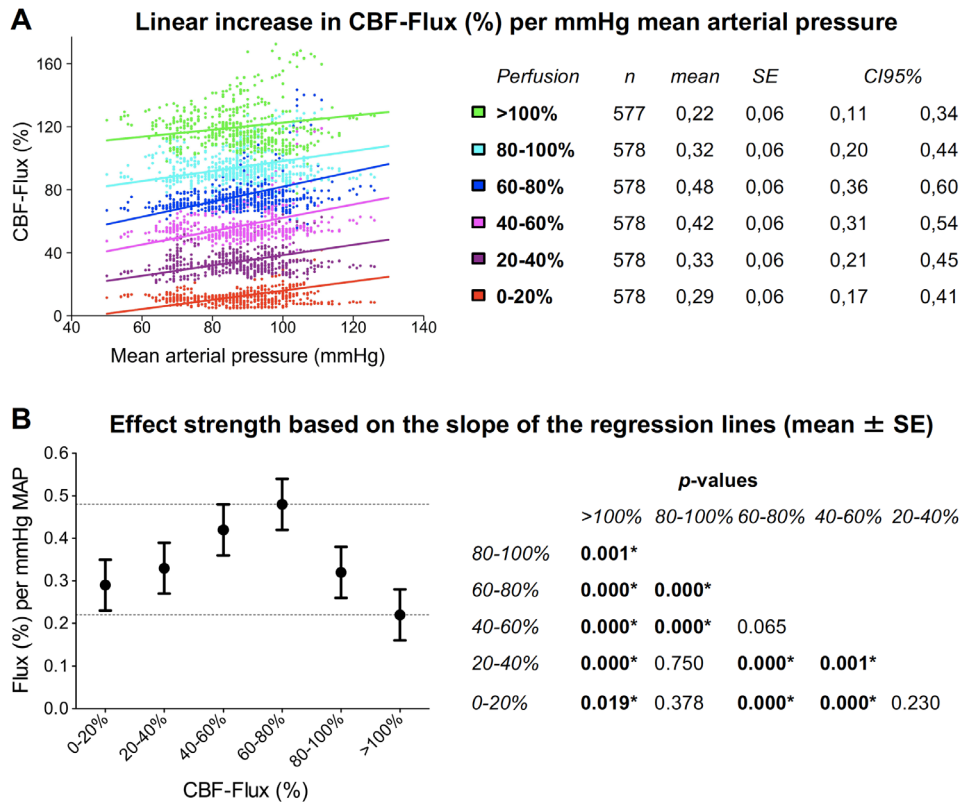
very low BP levels are harmful and associated with worse outcome.[37,38] One of the main concepts to guide BP management in critically ill patients follows the idea to maintain an individually optimal level of CPP, but

A **Linear increase in CBF-Flux (%) per mmHg mean arterial pressure**

Perfusion	n	mean	SE	CI95%	
>100%	577	0,22	0,06	0,11	0,34
80-100%	578	0,32	0,06	0,20	0,44
60-80%	578	0,48	0,06	0,36	0,60
40-60%	578	0,42	0,06	0,31	0,54
20-40%	578	0,33	0,06	0,21	0,45
0-20%	578	0,29	0,06	0,17	0,41

B **Effect strength based on the slope of the regression lines (mean ± SE)**

p-values

	>100%	80-100%	60-80%	40-60%	20-40%
80-100%	0.001*				
60-80%	0.000*	0.000*			
40-60%	0.000*	0.000*	0.065		
20-40%	0.000*	0.750	0.000*	0.001*	
0-20%	0.019*	0.378	0.000*	0.000*	0.230

FIGURE 4: (A) Dot plot of the arbitrary CBF-Flux according to the mean arterial pressure (MAP) during the 20-minute LSI monitoring period at a low frequency sampling rate of 0.02 Hz for illustration of the linear relationship between cortical perfusion and MAP for each perfusion category. The overall CBF-Flux/MAP sample size and mean slope of the regression lines are given on the right. (B) The mean slope of the regression lines (=linear increase in CBF-Flux [%] per mmHg MAP) is plotted for each perfusion category to show the strength of the association between CBF-Flux and MAP for each perfusion level. Significant differences between the mean slopes are indicated in bold (*right panel*). The level of significance for each comparison was Bonferroni adjusted to α = 0.003. In areas with perfusion patterns between 40% and 80%, perfusion changes per mmHg MAP were significantly greater than in areas with more likely infarcted (0–40%) or noninfarcted (80 ≥ 100%) tissue, indicating greater impairment of cerebral autoregulation. CBF = cerebral blood flow; CI = confidence interval; LSI = laser speckle imaging. [Color figure can be viewed at www.annalsofneurology.org]

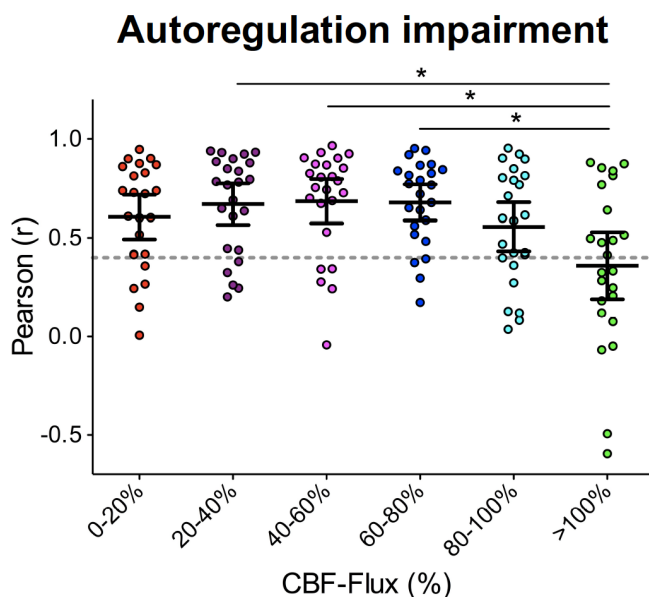## Autoregulation impairment

FIGURE 5: Autoregulation impairment calculated as a Pearson correlation of CBF-Flux and MAP for each perfusion category in all patients. The dashed gray line indicates our defined threshold of impaired autoregulation above r = 0.4. Correlation coefficients are presented as mean ± 95% CI. *$p < 0.05$; 1-way ANOVA with Bonferroni correction. ANOVA = analysis of variance; CBF = cerebral blood flow; CI = confidence interval; MAP = mean arterial pressure. [Color figure can be viewed at www.annalsofneurology.org]

degree of CA impairment, which in our patients was randomly spread across the hemisphere and determined at a perfusion level of 40 to 80%. Next to the underlying occlusion and reperfusion pattern of the ischemic stroke, this heterogenous distribution of CA impairment could be influenced by cerebrovascular collateralization, because LSI findings in experimental stroke have shown that BP elevation can rapidly increase blood flow both in the core and within the penumbra, prevent expansion of the blood flow deficit, and diminish the inverse blood flow response to spreading depolarization.[41] This appears in line with our observation of global CA impairment using iLSI in humans and suggests that CA impairment may serve as a mechanism to harness collateral recruitment as a bridging therapy in ischemic stroke.

An explanation for the link between the cortical perfusion level and degree of CA impairment could be the perfusion-dependent accumulation of cytotoxic metabolites and tissue acidosis, which correlates with the degree of CA impairment in the acute phase of large ischemic stroke.[6,42] The fact that CA impairment in tissue with perfusion levels at or above 100% was significantly less supports this hypothesis and, consequently, extended neuromonitoring – including parenchymal microdialysis – should be considered at the earliest possible timepoint to permit rapid identification of impaired autoregulation

patterns the moment they occur within tissue at highest risk for secondary neurological injury and infarct progression. Notably, our finding of increasingly normal CA along the gradient from low to increasingly higher perfusion also corresponds to the profound changes that the spreading depolarization continuum and its associated hemodynamic responses undergo from the core to increasingly well perfused tissue.[43] Fittingly, in patients with traumatic brain injury, it could be shown directly that normal CA was associated with normal and disturbed CA with an inverse hemodynamic response to spreading depolarization.[44]

Taken together, our findings argue for a more differentiated approach toward effective CA monitoring and highlight the importance to identify and target tissue regions with critically reduced perfusion levels and highest CA impairment before implantation of multimodal neuromonitoring probes. In patients requiring open surgery, distinction of critical hypoperfusion can be done with intraoperative optical imaging. In patients not requiring surgery, high-resolution CT-based or MR-based cerebral perfusion imaging could help identify ROIs with critically reduced perfusion and permit stereotactic implantation of neuromonitoring probes using image guidance technology.

Limitations

A technical limitation of this study is that our setup for arterial BP recording and CBF-Flux assessment required 2 separate measurement and recording modalities that do not allow synchronous recording of BP and CBF-Flux waveforms, like established solutions for multimodal bedside neuromonitoring.[45] Naturally, this restricts a more detailed and high-resolution analysis of the temporal association between BP fluctuations and the cerebral perfusion changes that we noted. Second, intraoperative iLSI provides no direct information on tissue integrity. This represents a limitation, because CPP-based treatment strategies targeting penumbral perfusion patterns are useless if the underlying tissue is already infarcted. To get a better understanding of our findings in the context of tissue integrity and perfusion, we superimposed the extent of the cortical infarction onto the iLSI perfusion maps in a subgroup of patients that received early postoperative MRI. Under exclusion of significant perfusion/diffusion mismatch at the timepoint of MRI, brain tissue viability did not influence the degree of CA impairment in areas with greatest CA impairment and critical perfusion patterns, which underlines that CA impairment appears to depend more on the regional perfusion level than on the underlying brain tissue viability itself. Third, it was previously shown in a noninjured rodent model that the occurrence of spreading depolarization did not affect the physiological
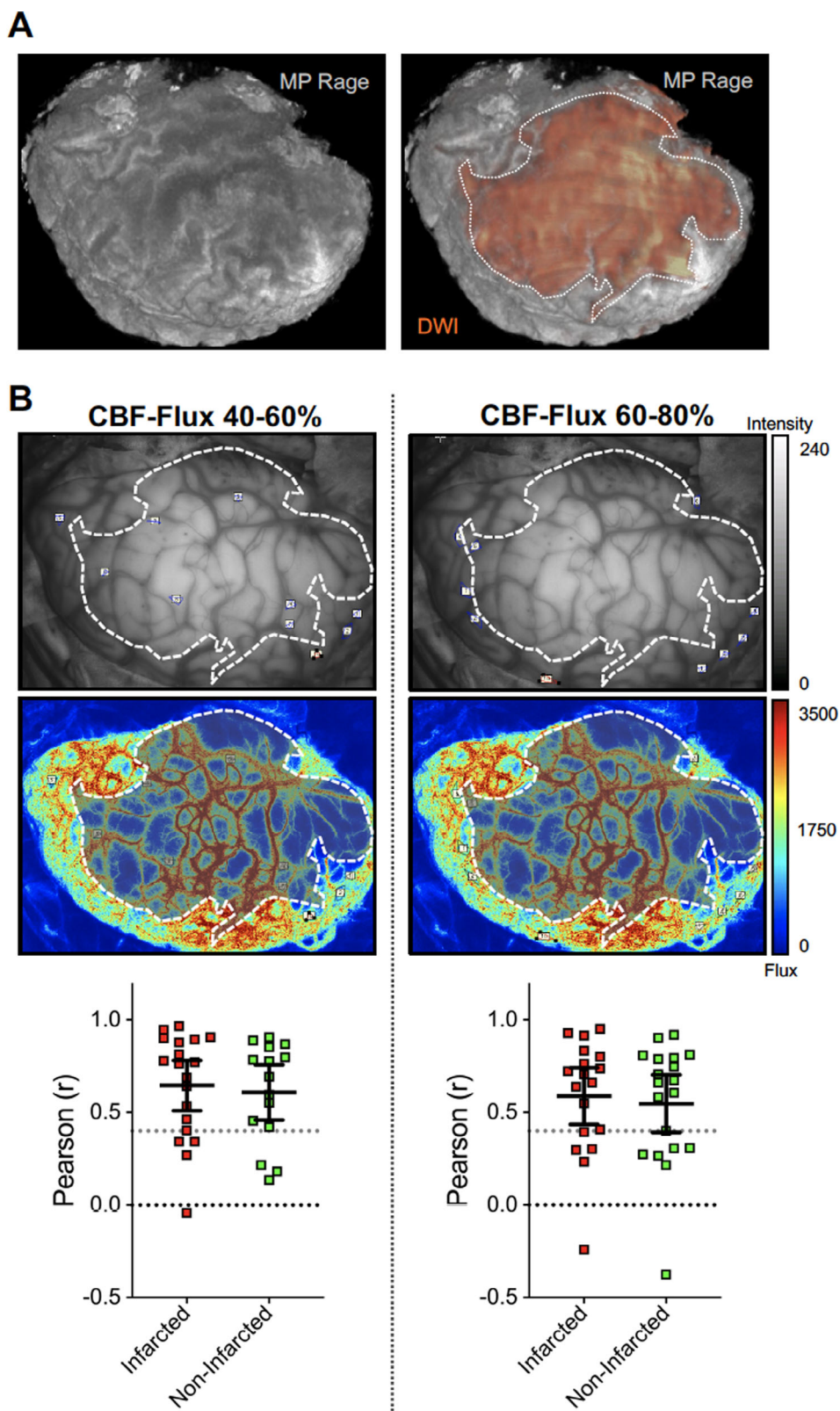
FIGURE 6: (A) Three-dimensional cortical surface reconstructions from the MP-RAGE data set of the postoperative MRI with overlay of the cortical infarct extension according to the DWI signal change in Patient number 20. (B) Corresponding screenshots of gray-scale raw speckle images and blood flow maps with overlay of the DWI infarct extension show the positioning of the ROIs for assessment of the 40 to 60% (left) and 60 to 80% (right) perfusion levels. The graphs illustrate the degree of autoregulation impairment depending on ROI localization in infarcted (red) or noninfarcted (green) tissue for 19 patients. The dashed gray line indicates a threshold of impaired autoregulation above r = 0.4. Correlation coefficients are presented as mean ± 95% CI. CBF = cerebral blood flow; CI = confidence interval; DWI = diffusion weighted imaging; MRI = magnetic resonance imaging; ROIs = regions of interest.

cerebrovascular perfusion response to changes in MAP.[46] In acute brain injury, however, the hemodynamic response to spreading depolarization is highly variable and particularly in ischemic stroke, the spatial–temporal influence of the spreading depolarization propagation pattern on CA remains unknown. Of course, spontaneous spreading depolarization that occurs at the infarct border and in areas of nonterminal infarction could have influenced CA within our ROIs, because the hemodynamic change associated with spreading depolarization propagates across the cortex and there appears to be a perfusion-dependent shift along the spreading depolarization-continuum toward persistent depolarization with sustained hypoperfusion in tissue with already critically reduced perfusion levels.[19,47–49]

Although we observed hemodynamic spreading depolarization propagation patterns in 4 patients, however, for the following reasons we decided to omit these propagation patterns in the context of our present analysis. First, persistent depolarization with sustained hypoperfusion was not noted[19] and the cortical surface affected by spreading depolarization propagation represented less than 1% of the cumulative exposed cortical surface area. Second, spreading depolarization-associated hemodynamic propagation patterns were generally rare and, if they occurred, then just briefly and not during the entire monitoring period.[19] Third, spreading depolarization propagation could have occurred directly before the start of our iLSI recording and remained undetected so that ultimately our setup did not permit us to draw a reliable conclusion regarding the effect of spreading depolarization propagation on CA.

Author Contributions

N.H. and J.W. contributed to the conception and design of the study. N.H., M.S., K.N., M.M., J.D., P.V., and J.W. contributed to acquisition and analysis of the data. N.H., M.S., and J.W. contributed to drafting the text and preparing the figures.

Potential Conflicts of Interest

The authors declared no conflict of interest.

References

1. Lassen NA. Cerebral blood flow and oxygen consumption in man. Physiol Rev 1959;39:183–238.

2. Lassen NA. Control of cerebral circulation in health and disease. Circ Res 1974;34:749–760.

3. Czosnyka M, Smielewski P, Kirkpatrick P, et al. Monitoring of cerebral autoregulation in head-injured patients. Stroke 1996;27:1829–1834.

4. Immink RV, Van Den Born BJH, Van Montfrans GA, et al. Impaired cerebral autoregulation in patients with malignant hypertension. Circulation 2004;110:2241–2245.

5. Jaeger M, Soehle M, Schuhmann MU, Meixensberger J. Clinical significance of impaired cerebrovascular autoregulation after severe aneurysmal subarachnoid hemorrhage. Stroke 2012;43:2097–2101.

6. Dohmen C, Bosche B, Graf R, et al. Identification and clinical impact of impaired cerebrovascular autoregulation in patients with malignant middle cerebral artery infarction. Stroke 2007;38:56–61.

7. Czosnyka M, Miller C, Le Roux P, et al. Monitoring of cerebral autoregulation. Neurocrit Care 2014;21:95–102.

8. Intharakham K, Beishon L, Panerai RB, et al. Assessment of cerebral autoregulation in stroke: a systematic review and meta-analysis of studies at rest. J Cereb Blood Flow Metab 2019;39:2105–2116.

9. Tiecks FP, Lam AM, Aaslid R, Newell DW. Comparison of static and dynamic cerebral autoregulation measurements. Stroke 1995;26:1014–1019.

10. Hecht N, Fiss I, Wolf S, et al. Modified flow- and oxygen-related autoregulation indices for continuous monitoring of cerebral autoregulation. J Neurosci Methods 2011;201:399–403.

11. Lang EW, Mehdorn HM, Dorsch NWC, Czosnyka M. Continuous monitoring of cerebrovascular autoregulation: a validation study. J Neurol Neurosurg Psychiatry 2002;72:583–586.

12. Zweifel C, Castellani G, Czosnyka M, et al. Continuous assessment of cerebral autoregulation with near-infrared spectroscopy in adults after subarachnoid hemorrhage. Stroke 2010;41:1963–1968.

13. Jaeger M, Schuhmann MU, Soehle M, Meixensberger J. Continuous assessment of cerebrovascular autoregulation after traumatic brain injury using brain tissue oxygen pressure reactivity. Crit Care Med 2006;34:1783–1788.

14. Paulson OB, Strandgaard S, Edvinsson L. Cerebral autoregulation. Cerebrovasc Brain Metab Rev 1990;2:161–192.

15. Xiong L, Liu X, Shang T, et al. Impaired cerebral autoregulation: measurement and application to stroke. J Neurol Neurosurg Psychiatry 2017;88:520–531.

16. Immink RV, Van Montfrans GA, Stam J, et al. Dynamic cerebral autoregulation in acute lacunar and middle cerebral artery territory ischemic stroke. Stroke 2005;36:2595–2600.

17. Powers WJ, Videen TO, Diringer MN, et al. Autoregulation after ischaemic stroke. J Hypertens 2009;27:2218–2222.

18. Hecht N, Woitzik J, König S, et al. Laser speckle imaging allows real-time intraoperative blood flow assessment during neurosurgical procedures. J Cereb Blood Flow Metab 2013;33:1000–1007.

19. Woitzik J, Hecht N, Pinczolits A, et al. Propagation of cortical spreading depolarization in the human cortex after malignant stroke. Neurology 2013;80:1095–1102.

20. Hecht N, Woitzik J, Dreier JP, Vajkoczy P. Intraoperative monitoring of cerebral blood flow by laser speckle contrast analysis. Neurosurg Focus 2009;27:E11.

21. Hecht N, Muller M-M, Sandow N, et al. Infarct prediction by intraoperative laser speckle imaging in patients with malignant hemispheric stroke. J Cereb Blood Flow Metab 2016;36:1022–1032.

22. Parthasarathy AB, Weber EL, Richards LM, et al. Laser speckle contrast imaging of cerebral blood flow in humans during neurosurgery: a pilot clinical study. J Biomed Opt 2010;15:66030.

23. Klijn E, Hulscher HC, Balvers RK, et al. Laser speckle imaging identification of increases in cortical microcirculatory blood flow induced by motor activity during awake craniotomy. J Neurosurg 2013;118: 280–286.

24. Vahedi K, Hofmeijer J, Juettler E, et al. Early decompressive surgery in malignant infarction of the middle cerebral artery: a pooled analysis of three randomised controlled trials. Lancet Neurol 2007;6: 215–222.

25. Juttler E, Unterberg A, Woitzik J, et al. Hemicraniectomy in older patients with extensive middle-cerebral-artery stroke. N Engl J Med 2014;370:1091–1100.

26. Zweckberger K, Juettler E, Bosel J, Unterberg WA. Surgical aspects of decompression craniectomy in malignant stroke: review. Cerebrovasc Dis 2014;38:313–323.

27. Neugebauer H, Fiss I, Pinczolits A, et al. Large size hemicraniectomy reduces early herniation in malignant middle cerebral artery infarction. Cerebrovasc Dis 2016;41:283–290.

28. Guresir E, Vatter H, Schuss P, et al. Rapid closure technique in decompressive craniectomy. J Neurosurg 2011;114:954–960.

29. Czosnyka M, Brady K, Reinhard M, et al. Monitoring of cerebrovascular autoregulation: facts, myths, and missing links. Neurocrit Care 2009;10:373–386.

30. Jaeger M, Schuhmann MU, Soehle M, et al. Continuous monitoring of cerebrovascular autoregulation after subarachnoid hemorrhage by brain tissue oxygen pressure reactivity and its relation to delayed cerebral infarction. Stroke 2007;38:981–986.

31. Chi NF, Hu HH, Wang CY, et al. Dynamic cerebral autoregulation is an independent functional outcome predictor of mild acute ischemic stroke. Stroke 2018;49:2605–2611.

32. Kiening KL, Unterberg AW, Bardt TF, et al. Monitoring of cerebral oxygenation in patients with severe head injuries: brain tissue PO2 versus jugular vein oxygen saturation. J Neurosurg 1996;85: 751–757.

33. Vajkoczy P, Roth H, Horn P, et al. Continuous monitoring of regional cerebral blood flow: experimental and clinical validation of a novel thermal diffusion microprobe. J Neurosurg 2000;93:265–274.

34. Ayata C, Dunn AK, Gursoy-Ozdemir Y, et al. Laser speckle flowmetry for the study of cerebrovascular physiology in normal and ischemic mouse cortex. J Cereb Blood Flow Metab 2004;24:744–755.

35. Dunn AK, Bolay H, Moskowitz MA, Boas DA. Dynamic imaging of cerebral blood flow using laser speckle. J Cereb Blood Flow Metab 2001;21:195–201.

36. Schmidt B, Czosnyka M, Raabe A, et al. Adaptive noninvasive assessment of intracranial pressure and cerebral autoregulation. Stroke 2003;34:84–89.

37. Ishitsuka K, Kamouchi M, Hata J, et al. High blood pressure after acute ischemic stroke is associated with poor clinical outcomes: Fukuoka stroke registry. Hypertension 2014;63:54–60.

38. Koton S, Eizenberg Y, Tanne D, Grossman E. Trends in admission blood pressure and stroke outcome in patients with acute stroke and transient ischemic attack in a National Acute Stroke registry. J Hypertens 2016;34:316–322.

39. Steiner LA, Czosnyka M, Piechnik SK, et al. Continuous monitoring of cerebrovascular pressure reactivity allows determination of optimal cerebral perfusion pressure in patients with traumatic brain injury. Crit Care Med 2002;30:733–738.

40. Czosnyka M, Hutchinson P, Smielewski P. Treatment targets based on autoregulation parameters in neurocritical care patients. Curr Opin Crit Care 2020;26:109–114.

41. Shin HK, Nishimura M, Jones PB, et al. Mild induced hypertension improves blood flow and oxygen metabolism in transient focal cerebral ischemia. Stroke 2008;39:1548–1555.

42. Woitzik J, Pinczolits A, Hecht N, et al. Excitotoxicity and metabolic changes in association with infarct progression. Stroke 2014;45: 1183–1185.

43. Dreier JP. The role of spreading depression, spreading depolarization and spreading ischemia in neurological disease. Nat Med 2011; 17:439–447.

44. Hinzman JM, Andaluz N, Shutter LA, et al. Inverse neurovascular coupling to cortical spreading depolarizations in severe brain trauma. Brain 2014;137:2960–2972.

45. Smielewski P, Lavinio A, Timofeev I, et al. ICM+, a flexible platform for investigations of cerebrospinal dynamics in clinical practice. Acta Neurochir Suppl 2008;102:145–151.

46. Lauritzen M. Long-lasting reduction of cortical blood flow of the rat brain after spreading depression with preserved autoregulation and impaired CO2 response. J Cereb Blood Flow Metab 1984;4: 546–554.

47. Dreier JP, Major S, Foreman B, et al. Terminal spreading depolarization and electrical silence in death of human cerebral cortex. Ann Neurol 2018;83:295–310.

48. Bere Z, Obrenovitch TP, Bari F, Farkas E. Ischemia-induced depolarizations and associated hemodynamic responses in incomplete global forebrain ischemia in rats. Neuroscience 2014;260:217–226.

49. Strong AJ, Anderson PJ, Watts HR, et al. Peri-infarct depolarizations lead to loss of perfusion in ischaemic gyrencephalic cerebral cortex. Brain 2007;130:995–1008.